Astron. Astrophys. 335, 183–198 (1998)

ASTRONOMY AND ASTROPHYSICS

The rotational velocity of low-mass stars in the Pleiades cluster⋆,⋆⋆

D. Queloz[1⋆⋆⋆], **S. Allain**[2], **J.-C. Mermilliod**[3], **J. Bouvier**[2], **and M. Mayor**[1]

[1] Observatoire de Genève, 51 ch. des Maillettes, CH-1290 Sauverny, Switzerland
[2] Laboratoire d"Astrophysique, Observatoire de Grenoble, Université Joseph Fourier, B.P. 53, F-38041 Grenoble Cedex 9, France
[3] Institut d'Astronomie de l'Université de Lausanne, CH-1290 Chavannes-des-bois, Switzerland

Received 13 January 1998 / Accepted 9 March 1998

Abstract. We present new $v \sin i$ measurements for 235 low-mass stars in the Pleiades. The differential rotational broadening has been resolved for all the stars in our sample. These results, combined with previously published measurements, provide a complete and unbiased rotation data set for stars in the mass range from 0.6 to $1.2 M_{\odot}$. Applying a numerical inversion technique on the $v \sin i$ distributions, we derive the distributions of *equatorial* velocities for low-mass Pleiades members. We find that half of the Pleiades dwarfs with a mass between 0.6 to $1\,M_{\odot}$ have rotation rates lower than $10\,\mathrm{km\,s^{-1}}$.

Comparison of the rotational distributions of low-mass members between IC 2602/2391 (≈ 35 Myr) and the Pleiades (≈ 100 Myr) suggests that G dwarfs behave like solid-bodies and follow Skumanich's law during this time span. However, comparison between Pleiades and older clusters –M34 (≈ 200 Myr) and Hyades (≈ 600 Myr)– indicates that the braking of slow rotators on the early main sequence is weaker than predicted by an asymptotical Skumanich's law. This strongly supports the view that angular momentum tapped in the radiative core of slow rotators on the zero age main sequence (ZAMS) resurfaces into the convective envelope between Pleiades and Hyades age. For the G-dwarfs, we derive a characteristic coupling time scale between the core and the envelope of about 100–200 Myr, which accounts for the observed evolution of surface rotation from the ZAMS to the Hyades.

The relationship between rotation and coronal activity in the Pleiades is in agreement with previous observations in other clusters and field stars. We show that the Rossby diagram provides an excellent description of the X–ray activity for all stars in the mass domain studied. The Pleiades data for slow and moderate rotators fills the gap between the X-ray–rotation correlation found for slow rotators and the X-ray "saturation plateau" observed for young fast rotators. The transition between increasing X-ray flux with rotation and X-ray saturation is observed at $\log(P/\tau) = 0.8 \pm 0.1$. These results strengthen the hypothesis that the "saturation" of the angular momentum loss process depends on the stellar mass.

Key words: stars: activity – stars: evolution – stars: pre-main sequence – Galaxy: open clusters and associations: Pleiades

1. Introduction

In the past 10 years, numerous rotational velocity measurements have been obtained for low-mass pre-main sequence stars and members of nearby young open clusters. This set of observations has shown that the angular momentum of each star follows an evolutionary scenario from the star's birth to the age of the Sun. Though several models have been developed to describe the rotational history of low-mass stars, the data available to confront models with observations were still insufficient to provide an unambiguous validation of these models. The measurements of stellar rotation for various ages and the understanding of its evolution shall provide a way to get a better knowledge of the physical processes experienced by the star through its history. In particular, this data might offer additional insight into the physics of young stars and their interactions with their protostellar and maybe their proto-planetary disks.

On the ZAMS, G type stars ($0.8 - 1.0 M_{\odot}$) exhibit a large spread of rotational velocities. A difference of the order of $150\,\mathrm{km\,s^{-1}}$ is observed for G dwarfs in Alpha Per (≈ 50 Myr) between the fastest and slowest rotators (Prosser 1992). At Hyades age (about 600 Myr), the spread has disappeared and the stars with masses in the 0.6 to $1\,M_{\odot}$ range show a monotically decreasing rotational velocity with mass (Radick et al. 1987; Stauffer et al. 1997a). Over this time span, the fast rotators have been strongly braked but the slow rotators have only suffered a little braking. Moreover, the efficiency of the braking process also depends on the stellar mass. At the Pleiades age (≈ 100 Myr), almost all G type stars have converged down to slow rotation while K dwarfs stars still exhibit a large rotational spread (Mayor & Mermilliod 1991; Soderblom et al. 1993). At the Hyades age, a significant spread in rotational velocity spread is only observed for stars less massive than $0.6 M_{\odot}$ (Stauffer et al. 1997a).

Send offprint requests to: Didier.Queloz@obs.unige.ch

⋆ Based on observations collected at the Observatoire de Haute-Provence with ELODIE at the 193cm telescope and with CORAVEL at the 1m-swiss telescope

⋆⋆ Tables 3,4,5 are also available in electronic form at the CDS via anonymous ftp 130.79.128.5

⋆⋆⋆ Present address: Jet Propulsory Laboratory, Mail-Stop: 306-473, 4800 Oak Grove Drive, Pasadena, CA 91109, USA

Models have difficulties to simultaneously reproduce the large diversity of rotators at early ages and their strong convergence in a few 100 Myr years. The recent discovery of a bi-modal velocity distribution for pre-main sequence stars in Taurus and Orion (see Bouvier 1994; Choi & Herbst 1996) suggests that the magnetic coupling between the disk and the star (Camenzind 1990; Königl 1991) could prevent the young star from spinning up during its PMS contraction, yielding a large spread in the initial angular momentum distribution. On the main sequence, the star's rotation is mostly ruled by the angular momentum losses at the surface through a magnetized wind (Schatzmann 1962; Weber & Davis 1967) and by the angular momentum transfer in the inner parts of the star (Endal & Sofia 1978; Mac Gregor & Brenner 1991). Depending on the efficiency of the transfer and the disk lifetime, various scenarios can be predicted. The latest models of angular momentum evolution are from Krishnamurthi et al. (1997a), Bouvier et al. (1997b) and Allain (1998).

Numerous data on stellar rotation were available to these models, though not enough yet to derive the complete distributions of rotational velocity in young open clusters. The comparison between such distributions and the initial velocity distribution gathered from T Tauri observations would provide an important additional constraint on the models.

Unbiased rotational velocity distributions are hard to build, numerous observations being needed to get a statistically significant distribution. In this case, measurements of the projected velocity ($v \sin i$) are a good alternative to the direct measurement of rotation periods which requires a huge number of photometric measurements, difficult to achieve for a large sample of stars. Indeed, since the pioneering work of van Leeuwen & Alphenaar (1982), there have been several attempts to measure photometric periods in the Pleiades (see O'Dell et al. 1995 for a census of the observations; Krishnamurthi et al. 1997b). Up to now, 42 periods have been measured in this cluster, for stars with $(B-V)_0$ in the range 0.5 to 1.4. The detection of rotational periods for the whole sample of Pleiades stars in this mass range (more than 200 catalogued members) is difficult and will still take a few years.

Measurements of $v \sin i$ are more straighforward but are obviously affected by projection effects. Yet, the knowledge of the $v \sin i$ for a large stellar sample does provide rich *statistical* information. It is then possible to extract an accurate estimate of the distribution of *equatorial* velocities in a cluster from a large number of observed *projected* rotational velocities if the stellar sample is statistically representative of the stellar population of the cluster and if it does not suffer from incompleteness (i.e., all the $v \sin i$ must be resolved). We consider that the inclination angles are randomly distributed in clusters.

In the next section we present new $v \sin i$ measurements for 235 Pleiades low-mass members. We show that by taking into account the spectral type of stars, we can calibrate the intrinsic width of the spectral lines and measure the $v \sin i$ of very slow rotators down to 1.5 km s^{-1}. The calibration process is described in Sect. 2. We detect rotational broadening for all observed stars. More than 98% Pleiades members of the original Hertzprung sample now have a resolved rotational velocity measurement up to $(B-V)_0$=1.35. The distributions of projected rotational velocities are then converted into distributions of equatorial velocities using a numerical algorithm described in Sect. 3. The velocity distributions for various mass ranges are presented in Sect. 4. In Sect. 5 we compare our results with those obtained for other open clusters and discuss the implications for the models of angular momentum evolution. We also examine the relationship between X-ray flux and stellar rotation for Pleiades stars.

2. The $v \sin i$ measurements

The ultimate technique to measure projected equatorial rotational velocity ($v \sin i$) is certainly the Fourier transform technique (Smith & Gray 1976) if the signal–to–noise of the spectra is high. The apparent magnitude of low mass stars in the Pleiades is however too faint for using such a technique. Cross-correlation algorithms which concentrate the spectral information have to be used. They allow us to measure the mean broadening of lines with a high precision even from low signal-to-noise spectra (Queloz 1995 and references herein). This technique is very efficient for F, G and K stars with slow and moderate rotation rates: applied to high resolution spectra covering a large wavelength range, it is known to yield projected rotational velocity with a precision of the order of 1 km s^{-1} for slow rotators (Benz & Mayor 1981, 1984).

For this study we used the CORAVEL (Baranne et al. 1979) and ELODIE (Baranne et al. 1996) spectrographs. CORAVEL is equipped with a mask, located in its focal plane. It builds cross-correlation functions by "optical" ways. ELODIE is the fiber-fed echelle spectrograph of the 193cm-telescope of the Haute-Provence Observatory. The echelle spectra are recorded on a 1024x1024 CCD and the cross-correlation functions are computed by an automatic reduction carried out directly after the observations using a K0 spectral type template (see Baranne et al. 1996 for details about the reduction process).

Although the way to compute the cross-correlation functions is different for both instruments, the algorithm is similar. They both yield Gaussian shaped cross-correlation functions whose interpretation is straightforward and perfectly fitted for rotation analysis. In both cases, the width of the cross-correlation function is estimated by fitting a Gaussian function. The accuracy of ELODIE observations is better than those of CORAVEL due to its higher spectral resolution but the $v \sin i$ measurements of both instruments are in good agreement (see below).

The mean broadening measured by the cross-correlation technique includes all intrinsic sources of line broadening such as micro and macroturbulence, pressure and magnetic Zeeman splitting. Therefore, the differential broadening of the cross-correlation function between two stars cannot directly be interpreted as only an effect of rotational broadening. This is probably the main limit to the accuracy of the $v \sin i$ determinations for slow rotators. However, the calibration of the $v \sin i$ carried out for ELODIE (see below) and those of Benz & Mayor (1984) for CORAVEL shows that a reliable interpretation of the differ-

ential broadening as a projected rotation velocity for F, G and K dwarf stars is possible down to a value of $2\,\mathrm{km\,s^{-1}}$ if both the spectral type and metallicity of stars are taken into account. The derivation of the rotational velocity distribution free of systematic effects through a range of mass for open cluster stars is thus possible.

2.1. Calibration of the ELODIE $v \sin i$ for slow rotating dwarf stars

The effect of stellar rotation on the spectral lines can be fairly well approximated by a convolution between a non-rotating spectrum and the analytical broadening function described in Gray (1976). This function, which only takes into account the geometrical effect of a solid body rotation and the center-to-limb darkness effect, is accurate enough for slow rotator measurements considering the uncertainties on the intrinsic widths of stellar spectral lines. Compared to a complete treatment with integration of spectra on a grid, this approximation leads to errors less than $1\,\mathrm{km\,s^{-1}}$ (Benz & Mayor 1981, Marcy & Chen 1992). In comparison the uncertainties in the knowledge of intrinsic widths of the cross-correlation reach $1.5\,\mathrm{km\,s^{-1}}$ (see below).

In the slow rotator domain, up to $v \sin i$ $20\,\mathrm{km\,s^{-1}}$, with our spectral resolution, the shape of the cross-correlation function is very well approximated by a Gaussian. Therefore, the effect of the rotationnal broadening can be expressed as a quadratic broadening of the cross-correlation function:

$$v \sin i = A\sqrt{\sigma^2 - \sigma_0^2}, \tag{1}$$

where σ is the observed width, σ_0 the intrinsic width (no rotation) and A the constant coupling the differential broadening of the cross-correlation functions to the $v \sin i$ of stars. With a sample of non-rotating stars ranging from G5 to M0 (see in Table 2 for references), a mean value for A is measured. The result of the computation of the A constant from various non-rotating dwarf stars artificially broadened up to $20\,\mathrm{km\,s^{-1}}$ is listed in Table 1. In this rotation domain no difference greater than $0.3\,\mathrm{km\,s^{-1}}$ has been measured between the quadratic broadening model (Eq. 1) and the input rotation. A mean value of $A = 1.9 \pm 0.1$ is used in this work.

The parameter σ_0 represents the mean intrinsic width for non-rotating stars. It depends on the instrumental profile and all intrinsic broadening phenomena affecting the spectral lines. Its precise knowledge is crucial to measure slow rotators below $5\,\mathrm{km\,s^{-1}}$.

2.1.1. The intrinsic width of the cross-correlation function

ELODIE is an extremely stable instrument. It is kept in an isolated room with a temperature control and is fed by optical fibers. The instrumental profile is therefore very stable from one run to the other. In order to measure the value of the σ_0 parameter for a mass domain from $1.2\,\mathrm{M_\odot}$ to $0.5\,\mathrm{M_\odot}$, a set of non-rotating dwarf stars has been observed ranging from G0 to M0 (Table 2). With the reasonable assumption that all non-rotating stars with the same temperature and the same metallicity share similar intrinsic broadenings, this set of stars yields the following calibration (see Fig. 1):

$$\sigma_0 = 0.27(\mathrm{B-V})^2 + 4.51\ (\pm 0.06)\ (\,\mathrm{km\,s^{-1}}\,). \tag{2}$$

The $60\,\mathrm{m\,s^{-1}}$ typical uncertainty on the individual broadening of cross-correlation functions of each star yields a $1.5\,\mathrm{km\,s^{-1}}$ lower limit for $v \sin i$ measurements by our technique. It is worth stressing that such uncertainty has little impact on the $v \sin i$ measurements of rotators faster than $3\,\mathrm{km\,s^{-1}}$ (see Fig. 1).

This calibration is also limited to stars with solar metallicities. In particular the intrinsic widths of cross-correlation functions for stars HD 10700 and HD 190007 differ significantly from those of other stars having a similar temperature because of their specific metallicity content. The star HD 10700 is a metal poor star ([Fe/H]=–0.57 from Arribas & Crivellari 1989) and the star HD 190007 belongs to the "super-metal-rich" class stars (Taylor& Johnson 1987). All the other calibration stars have solar type metallicities. Since a rise of metallicity increases the number of saturated lines, the mean spectral width, seen by the correlation process, is slightly broadened. A diminution of the stellar metallicity content induces the opposite effect. The use of the above calibration for deficient and metal-rich stars would induce, respectively, a systematic $v \sin i$ underestimation and a systematic $v \sin i$ over-estimation.

We selected the same kind of analytical function as those used by Benz & Mayor (1994) to model the σ_0 change versus B–V. Such a choice already proved to be fairly good. We decided that the correction for high rotators included by Benz & Mayor (1984) was not worth adding to our ELODIE σ_0 calibration considering the small rotational velocities of our program stars. The calibration found for ELODIE is very close to the CORAVEL one. A rescaling of the ELODIE result (Eq. 2) to CORAVEL resolution ($\sigma^2(\mathrm{CORAVEL}) = \sigma^2(\mathrm{\ ELODIE}) + (5.15)^2$) leads to $\sigma_0 = 6.85 + 0.177(\mathrm{B-V})^2$, which is close to the direct Benz & Mayor (1984) calibration.

Various effects can produce the observed broadening of the cross-correlation function with the increase of B−V value of

Table 1. A constant computed with various non-rotating dwarf stars artificially broadened up to $20\,\mathrm{km\,s^{-1}}$.

Name	B–V	A
HD 115641	0.7	1.99
HD 185144	0.8	1.86
HD 10476	0.84	1.98
HD 4628	0.88	1.96
HD 16169	0.95	1.93
HD 190007	1.15	1.85
HD 201092	1.37	1.86
mean value		1.92

Table 2. Observed ELODIE cross-correlation width for a set of non-rotating stars. Column number: (3) $v \sin i$ from (a) Soderblom 1983 and (b) Gray 1984 (spectroscopic determination), (c) Noyes et al. 1984 (estimation from S index), (d) Baliunas et al. 1983 (estimation from rotation period); (4) width of the ELODIE cross-correlation function; (5) ELODIE $v \sin i$ (computed with Eq. 1 and 2). The $v \sin i$ values less than zero are artifacts due to uncertainties in the width measurement. The two stars with an asterisk which differ from the calibration are discussed in the text (see Sect. 2.1.1).

Name	B–V	$v \sin i$ other $\mathrm{km\,s^{-1}}$	σ $\mathrm{km\,s^{-1}}$	$v \sin i$ ELODIE $\mathrm{km\,s^{-1}}$
(1)	(2)	(3)	(4)	(5)
HD 109358	0.59	1.8[a]	4.793	2.5 ± 0.5
Sun	0.64	2.0	4.698	1.6 ± 0.7
HD 32923	0.65	1.6[a]	4.720	1.8 ± 0.6
HD 217014	0.67	1.7[a]	4.793	2.3 ± 0.5
HD 115617	0.71	0.0[b]	4.685	1.1 ± 1.0
HD 10700⋆	0.72	0.9[b]	4.563	-1.7 ± 0.6
HD 185144	0.80	0.4[b]	4.635	-1.3 ± 0.9
HD 26965	0.82	1.0[c]	4.750	1.1 ± 1.0
HD 10476	0.84	0.9[c]	4.677	-0.9 ± 1.2
HD 3651	0.85	0.7[d]	4.680	-0.9 ± 1.2
HD 166620	0.87	0.8[d]	4.681	-1.0 ± 1.1
HD 4628	0.88	0.9[d]	4.735	0.7 ± 1.5
HD 16160	0.95	0.7[d]	4.758	1.3 ± 0.9
HD 160346	0.95	1.0[d]	4.806	0.4 ± 1.7
HD 190007⋆	1.15	1.0[d]	5.023	2.4 ± 0.5
HD 201091	1.17	0.8[d]	4.980	1.9 ± 0.6
HD 201092	1.37	0.5[d]	5.031	0.7 ± 1.7

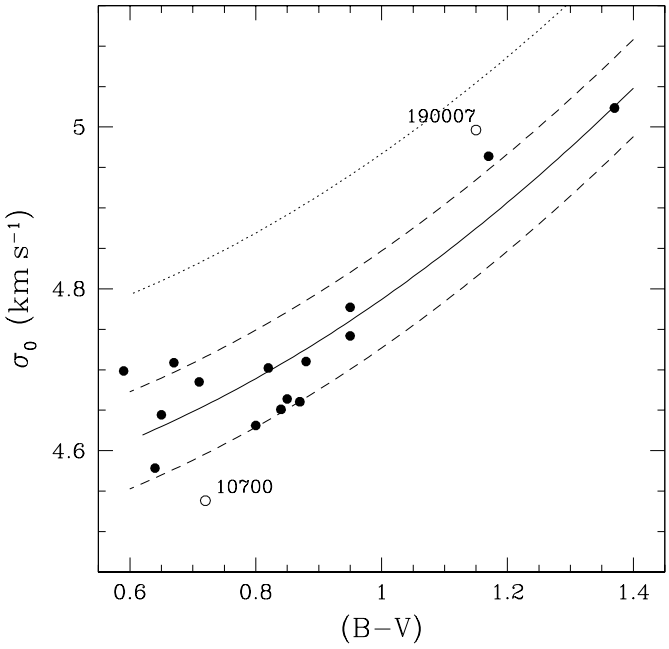

Fig. 1. Intrinsic width of the cross-correlation function (σ_0) vs $(B-V)$ for a sample of non-rotating dwarf stars. σ_0 is computed with Eq. 1 using column (3) and (4) of Table 2. The solid line is Eq. 2 (fitted without HD 10700 and HD190007 (open dots) values; see discussion in text). Dashed lines indicate a $60\,\mathrm{m\,s^{-1}}$ uncertainty on the knowledge of the intrinsic width of the cross-correlation function corresponding to $v \sin i$ $\pm 1.5\,\mathrm{km\,s^{-1}}$. The dotted line illustrates the σ-width of cross-correlation functions for stars with a rotation broadening $v \sin i = 3\,\mathrm{km\,s^{-1}}$.

stars. We have first investigated an "instrumental effect" due to the cross-correlation technique itself. The resolution change of ELODIE through the wavelength domain is too small to have any significant effect. The cross-correlation function is the mean of spectral lines weighted by the continuum of spectrum. Since the template (or mask) optimization algorithm (Baranne et al. 1979) does not care about keeping a constant resolution through the wavelength domain, the relative weighting of lines (between blue lines and red lines) can affect the cross-correlation width. However the observed widths of the cross-correlation functions computed with the blue and the red domains of spectra do not differ significantly.

Benz & Mayor (1984) argued that an increase of magnetic field strength in K and M dwarf stars is one of possible causes of the broadening of the cross-correlation function of late type stars. Using a correlation technique with magnetically sensitive templates (see Queloz et al. 1996 for details) an upper limit of 1kG can be set on our late type non-rotating standard stars. With a 1.5kG mean magnetic field upper limit, a Zeeman quadratic broadening of less than $1.5\,\mathrm{km\,s^{-1}}$ is computed using a typical Landé factor $g_{\mathrm{eff}} = 1$ for the lines. Thus, in our case, the magnetic field is not strong enough to be responsible of the broadening of the cross-correlation function of our standard late type stars.

The change of damping coefficient value is probably the main cause of the observed line broadening of late type stars. For most lines in cool stars the pressure broadening is of Van Der Waal type. The behavior of the γ_6 damping constant related to this broadening mechanism can be approximated as follow: $\log(\gamma_6) \sim \log(P) - 0.7 \log(T)$ (Gray 1976). Therefore, when the temperature decreases the damping parameter becomes stronger and the spectral lines broader. Since the macroturbulence decreases with the temperature (Gray 1984), the competition between the pressure broadening and the macroturbulence effect could be responsible for the flattenning of the intrinsic broadening observed around B–V$= 0.6$.

2.2. Pleiades stars

The $v \sin i$ measurements of 139 Pleiades stars with $0.5 < (B-V)_0 < 1.4$ are listed in Table 3. Most of these stars previously had only $v \sin i$ upper limits (see Soderblom et al. 1993). These new data significantly increase the number of resolved rotators. In this color range, almost all Pleiades stars located in the center of the cluster now have a $v \sin i$ measurement.

In Table 4, CORAVEL measurements are listed for 82 corona stars recently selected as new Pleiades members by Rosvick

Table 3. CORAVEL and ELODIE $v \sin i$ measurements of Pleiades stars from the Hertzprung (1947) and Soderblom (1993) samples. Most of these stars had previously only $v \sin i$ upper limits. SB2 indicates a double line spectroscopic binary where the two components are unresolved. An extra "a" or "b" character added to the name of stars indicates each component of a SB2 system. The stars detected as "no dip" by CORAVEL are unresolved very fast rotators ($v \sin i > 60\,\mathrm{km\,s^{-1}}$).

star HII	B–V$_0$	$v \sin i$ (km s^{-1}) CORAVEL	ELODIE	star HII	B–V$_0$	$v \sin i$ (km s^{-1}) CORAVEL	ELODIE	star HII	B–V$_0$	$v \sin i$ (km s^{-1}) CORAVEL	ELODIE
25	0.443	44.2±4.9		793	1.378		5.0±0.8	1593	0.716	3.0±1.4	1.8±1.0
34	0.888	7.3±1.1	5.9±0.8	799	1.287		4.7±0.8	1613	0.494	20.1±0.8	
97	1.043		6.8±0.8	870	0.68		9.7±0.9	1726	0.505	12.9±0.7	
102	0.684	18.3±0.5		879	1.032	7.2±1.3	5.6±0.8	1756	1.325		5.0±0.8
120	0.666	9.4±1.2		882	1.040	no dip		1766	0.435	22.7±1.3	
129	0.830	5.3±1.4		883	1.086		3.8±0.8	1776	0.680	10.3±1.0	9.8±0.9
152	0.647	11.1±1.2	11.8±0.9	885	0.988	6.1±1.1	5.2±0.8	1785	1.361		6.5±0.8
164	0.459	38.9±5.1		890	1.344		5.4±0.8	1794	0.589	11.2±0.8	
173a	0.73	7.8±1.2		915	1.199		9.3±0.8	1797	0.515	19.6±0.9	
173b	0.83	6.3±2.2		916	0.824	6.7±1.0	5.6±0.8	1856	0.514	15.4±0.9	
174	0.811	no dip		923	0.579	18.2±0.6		1924	0.568	14.2±0.7	
186	0.76	11.1±0.7		974	1.288		4.2±0.8	2016	1.181		9.8±0.9
189	1.328		4.7±0.8	996	0.603	11.9±0.8		2027a	0.76	5.6±1.6	
191	1.36		9.1±0.8	1015	0.609	9.6±1.1		2106	0.823	3.7±1.5	8.0±0.8
193	0.758	6.3±1.4	6.8±0.8	1032	0.733	37.2±1.9		2126	0.815	2.6±1.7	5.3±0.8
233	0.493	14.1±0.7		1039	0.958	< 5	4.9±0.8	2147a	0.742	6.9±3.2	
248	0.738	12.1±1.1		1061	1.358		7.1±0.8	2147b	0.742	10.8±2.3	
250	0.637	6.9±1.1	5.9±0.8	1095	0.858	3.6±2.6	3.6±0.8	2172	0.582	10.3±0.4	
253	0.648	38.2±1.8		1100	1.088		5.4±0.8	2209	1.336		5.4±0.8
263	0.836	7.8±0.8		1101	0.572	SB2		2278	0.828	6.1±0.9	7.7±0.8
293	0.665	6.6±1.0	5.1±0.8	1110	1.170		5.9±0.8	2284	0.743	3.5±1.3	3.7±0.8
296	0.799	14.7±0.9		1114	1.357		7.3±0.8	2311	0.780	6.2±1.3	6.5±0.8
298	0.835	6.6±1.1	6.3±0.8	1117a	0.62	6.4±2.6		2341	0.672	3.4±1.7	3.6±0.8
303	0.856	17.4±0.7		1117b	0.67	3.6±2.5		2366	0.779	2.9±1.7	4.3±0.8
314	0.613	41.9±1.6		1122	0.425	28.6±1.2		2406	0.720	9.2±0.5	8.5±0.8
320	0.840	10.8±0.5		1124	0.924	5.6±3.3	3.5±0.8	2407†	0.910		6.3±0.8
338	0.428	$>$40		1132	0.451	$>$40		2462	0.791	5.4±1.2	4.9±0.8
345	0.806	18.9±0.7		1136	0.784	no dip		2500	0.58	33.0±3.4	
357	1.182		10.0±0.9	1139	0.437	31.4±1.9		2506	0.552	13.8±0.8	
380	1.171		6.0±0.8	1182	0.597	16.4±1.1		2548	1.297		5.7±0.8
405	0.495	18.2±1.0		1200	0.507	13.7±0.9		2588	1.133		5.2±0.8
430	0.777	7.3±1.0	6.3±0.8	1207	0.591	5.1±1.3		2644	0.698	3.6±1.9	5.0±0.8
451	1.169		5.7±0.8	1215	0.599	6.5±0.9	4.1±0.8	2665	0.790	5.9±1.2	5.4±0.8
476	0.53	21.0±1.0		1220	0.830	4.8±1.3	6.3±0.8	2741	0.972		7.8±0.8
489	0.594	18.3±0.8		1275	0.791	6.4±1.2	6.4±0.8	2786	0.562	22.0±1.0	
513	1.275		7.4±0.8	1298	0.957	5.6±2.2	4.8±0.8	2870	0.974		4.0±0.8
514	0.657	10.5±1.0		1332	0.988	< 2	5.3±0.8	2880	0.818	6.3±1.1	6.0±0.8
522	0.879	3.6±0.8	4.4±0.8	1348a	1.05		5.1±0.8	2881*	0.920	7.8±1.1	13.3±1.0
571	0.748	7.6±0.5	6.8±0.8	1348b	1.35		1.8±0.8	2984	0.961		5.4±0.8
590	1.323		6.9±0.8	1355	1.362		12.5±0.9	3019	1.174		6.0±0.8
627	0.473	33.2±1.3		1392	0.55	15.7±1.6		3096	0.948	6.2±1.3	
636	0.981		3.5±0.8	1454	1.068		3.3±0.8	3097	0.697	14.6±0.3	
659	0.66	12.2±1.1		1485	1.309		42.0±2.2	3104	1.24		7.1±0.8
676	1.065		5.5±0.8	1512	1.207		5.3±0.8	3179	0.529	5.5±1.2	4.3±0.8
727	0.519	$>$40		1514	0.609	13.6±0.8		3187	1.139		6.2±0.8
739	0.586	14.4±0.6		1516	1.267		105±10				
746	0.768	4.9±1.0	4.8±0.8	1553	1.078		9.6±0.9				

(†) Binary systems with rotations synchronized to the orbital motion.
(*) Suspected long period double line spectroscopic binary (unresolved).

et al (1992) and Mermilliod et al. (1997). This selection is based on proper motion, photometry and radial velocity measurements. For the corona stars selected on the basis of the van Leeuwen (1983) proper motion measurements, the probability to catch a non-member with a photometry and a proper motion in agreement with the Pleiades ones is 25% in a velocity range of 60 km s^{-1} around the Pleiades radial velocity (see the radial velocity distribution of non-members compared to that of members in Fig. 1 of Rosvick et al. 1992). For the selection of Mermilliod et al. (1997), based on Artjukhina et al. (1970) proper motions, we expect more contaminants (2-3 times greater) because the accuracy of the astrometry is not as good as that of van Leeuwen (1983). Since candidate members were selected over a radial velocity domain of ± 2 km s^{-1} (Rosvick et al. 1992) and ± 4 km s^{-1} (Mermilliod et al. 1997) around the cluster's mean radial velocity, and considering that the radial velocity of field stars is almost random around the cluster velocity, we may have perhaps 3–4 non-members hidden in our corona sample. Such a small number of contaminants does not have significant impact on the final rotation velocity distribution.

All the $v \sin i$ measurements done with CORAVEL are based on many observations spread over the past 15 years. In order to avoid any statistical bias in the measurement of the mean $v \sin i$ per star (Eq. 1 is highly non-symmetric when σ is close to σ_0), a weighted mean broadening (σ) was first computed for each star and then transformed into $v \sin i$ according to the Benz & Mayor (1981, 1984) calibration. To take into account the instrumental uncertainties due to the variation of the point spread function of CORAVEL from night to night and be consistent with the dispersion measured on the mean broadening (σ) of the cross-correlation function of each star, an internal error of 0.2 km s^{-1} has been added to the photon noise of each measurements. Most of the ELODIE $v \sin i$ are computed from only one spectrum. When two measurements were available we used the same procedure that for CORAVEL measurements but without any extra intrumental uncertainty since the stability of the mean width of point spread function of ELODIE proved to be better than ± 10 m s^{-1}. Both ELODIE and CORAVEL $v \sin i$ error bar estimates listed in this paper are in agreement with the internal errors displayed by the dispersion of individual measurements of each star.

The limited scanning domain of CORAVEL restricts the $v \sin i$ measurements to small and moderate rotators (< 40 km s^{-1}). The faster rotators only have $v \sin i$ *lower* limits. For very fast rotating stars (> 60 km s^{-1}), the cross-correlation function in the scanning domain is flat. The CORAVEL measurements of stars cooler than F2 spectral type and without dip detection (referred as "no dip" in the tables) corresponds to the detection of fast rotating stars. The limitation of the width of the CORAVEL scanning domain leads also to a slight over-estimation of the $v \sin i$ for rotators faster than 30 km s^{-1} (see Fig. 2). In that case, the width of the scanning window is too small to accurately measure the location of the continuum around the dip, and the Gaussian χ^2–fit is biased towards broader Gaussians. The $v \sin i$ measurement of fast rotators observed with ELODIE has been computed by searching for the best match between the observed cross-correlation functions and others computed from a non-rotating star artificially broadened by the Gray (1976) analytical function.

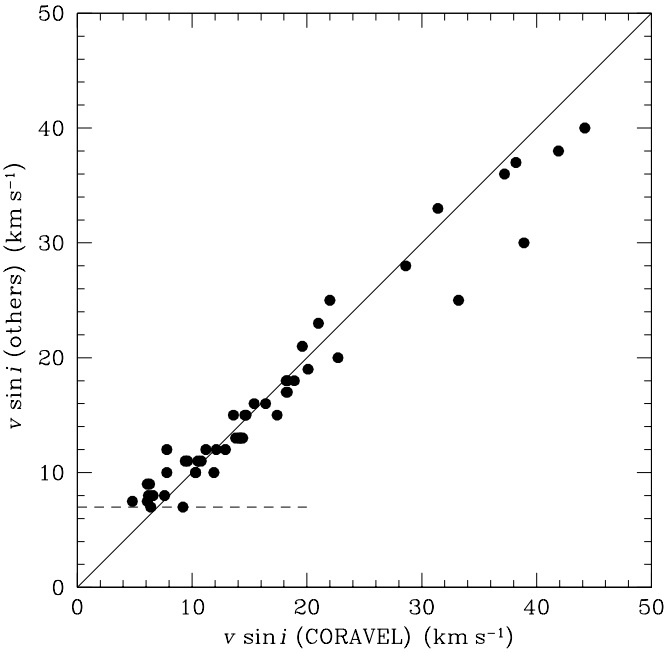

Fig. 2. The comparison between $v \sin i$ measurements from CORAVEL and from Soderblom et al. (1993) is displayed for common Pleiades stars. The dashed line indicates the lower limit for Soderblom et al. (1993) measurements. For rotators faster than 30 km s^{-1}, the CORAVEL measurements exhibit a slight deviation from the one-to-one relation displayed by the solid line. This effect is caused by the limited scanning domain of CORAVEL.

In Table 5, ELODIE measurements of 16 corona stars from Pels's list suspected to be members by van Leeuwen (1983) are displayed. All of these stars were selected as Pleiades members based on their photometry and proper motion. For all of them, we measure a radial velocity very close to the mean cluster velocity. By considering the size of the radial velocity selection window (± 1 km s^{-1}) and by following the same argument as above regarding the contamination by field stars, we do not expect any non-members to be hidden in this sample .

Some stars in our sample (HII 173, HII 1101, HII 1117, HII 1348, HII 2027, HII 2147, Pels 3, Ib 146, Ib 288, V 198) have been detected as double-lined spectroscopic binaries (SB2). For most of them we clearly resolved each component and we are able to measure their rotational broadening. Moreover, since we know their mass ratio either from the relative contrast of their cross–correlation function or from the orbit solution (when there is one), we can also estimated their $(B-V)_0$ and used that value to compute their $v \sin i$. Each of these measurements are identifed in Tables 3 and 4 with the standard notation used by spectroscopists for SB2 binaries. An extra "a" or "b" character has been added to the star name.

For all stars in common between CORAVEL and ELODIE observed samples, the comparison of the $v \sin i$ measurements shows a good agreement (see Fig. 3) with a difference

Table 4. CORAVEL $v \sin i$ measurement of stars located in the corona of the Pleiades and recently selected by Rosvick et al. (1992) and by Mermilliod et al. (1997) as cluster members.

star	(B−V)$_0$	$v \sin i$ (km s^{-1})	star	(B−V)$_0$	$v \sin i$ (km s^{-1})	star	(B−V)$_0$	$v \sin i$ (km s^{-1})
R60	0.440	no dip	Pels 39*	0.83	2.0±2.0	Pels 143	0.85	5.2±1.2
S151x	0.46	21.6±1.0	Pels 40	0.53	11.9±0.7	Pels 146	0.62	17.6±1.4
S183x	0.5	32.3±1.4	Pels 44	0.86	3.9±3.1	Pels 150	0.48	26.3±1.7
S37	0.403	no dip	Pels 45	0.78	7.8±1.3	Pels 151	0.67	5.5±2.2
S39	0.424	no dip	Pels 46	0.7	8.1±1.2	Pels 173	0.41	36.7±3.0
Pels 3	0.47	SB2	Pels 47	0.86	4.5±1.5	Pels 174	0.54	>40
Pels 4	0.78	2.6±1.7	Pels 50	0.8	7.0±1.5	Ia 317	0.5	>40
Pels 5	0.66	11.1±0.9	Pels 56	0.77	>40	Ib 038	0.66	10.9±0.9
Pels 6	0.47	35.9±3.1	Pels 60	0.52	no dip	Ib 055	0.74	6.6±1.0
Pels 7	0.62	2.7±1.9	Pels 68	0.81	6.7±2.0	Ib 078	1.03	6.4±1.1
Pels 8	0.64	15.5±1.0	Pels 69	0.81	16.3±0.8	Ib 146a	0.45	12.4±3.5
Pels 11	0.82	5.2±1.3	Pels 71	0.77	9.1±1.1	Ib 146b	0.5	8.6±5.3
Pels 12	0.69	11.2±0.9	Pels 75	0.87	>40	Ib 288	1.01	SB2
Pels 15	0.54	24.4±1.1	Pels 78	0.7	8.8±1.1	II 293	0.65	8.5±0.9
Pels 17	0.5	29.3±2.0	Pels 79	0.73	2.8±1.7	II 359	0.57	16.6±0.9
Pels 18	0.58	11.8±1.0	Pels 83	0.69	14.5±1.1	III 059	0.8	4.1±1.2
Pels 19	0.85	4.8±1.4	Pels 86	0.45	no dip	III 079	0.43	no dip
Pels 20	0.61	9.6±1.1	Pels 89	0.84	3.2±2.1	III 391	0.73	2.3±1.8
Pels 23	0.55	36.2±1.7	Pels 121	0.62	4.9±1.1	III 679	0.96	4.1±1.5
Pels 25	0.443	no dip	Pels 123	0.92	3.1±2.1	III 700	0.67	9.3±0.9
Pels 28	0.94	8.9±1.2	Pels 124	0.5	20.5±0.9	IV 131	0.77	2.2±1.5
Pels 29	0.6	33.8±1.9	Pels 126	0.58	9.8±1.0	IV 314	0.98	2.7±2.8
Pels 30	0.9	6.7±1.1	Pels 128	0.61	4.6±1.5	V 088	0.77	5.2±1.2
Pels 31	0.94	12.2±1.0	Pels 135	0.45	no dip	V 198a	0.6	10.5±1.1
Pels 34	0.69	3.6±1.4	Pels 137	1.01	3.6±1.6	V 198b	0.87	2.0±2.0
Pels 35	0.51	19.4±1.1	Pels 138	0.76	5.6±1.6	V 308	0.78	8.0±1.0
Pels 37	0.63	13.4±2.6	Pels 140	0.45	11.5±1.2			
Pels 38	0.73	3.1±2.0	Pels 142	0.81	3.9±1.5			

(*) Pels 39 lies slightly above the main sequence but doesn't show any hint of binarity with radial velocities. However, its very small $v \sin i$ value is an indication that this star could be a non-member.

Table 5. ELODIE $v \sin i$ and radial velocity (V_r) measurements of new members of the Pleiades corona. ($O-C$) is the velocity difference with the mean velocity of the cluster corrected from the projection effect. Note that, in order to use the convergent point measured by Rosvick et al. (1992) to compute the ($O-C$), the ELODIE measurements have been converted into the CORAVEL zero point reference frame. The following velocity offset has been used: $V_E - V_C = 0.48 - 1.45(B-V) + 0.53(B-V)^2$ (Udry et al. 1998).

star	(B−V)$_0$	$v \sin i$	V_r	$(O-C)$	star	(B−V)$_0$	$v \sin i$	V_r	$(O-C)$
Pels 9	1.0	5.5±0.8	6.41	−0.15	Pels 72	0.72	160±10	6.0:	0.78
Pels 22	0.90	12.1±0.9	5.08	0.34	Pels 109	1.31	5.5±0.8	4.96	−0.35
Pels 41	0.90	5.1±0.8	5.59	0.56	Pels 114	1.04	6.0±0.8	6.70	0.21
Pels 43	0.92	6.8±0.8	4.92	0.04	Pels 115	1.06	5.5±0.8	6.28	0.24
Pels 59	0.99	5.6±0.8	5.06	0.02	Pels 137	1.01	5.2±0.8	4.90	0.12
Pels 63	1.07	2.9±0.8	7.41	−0.36	Pels 162	0.91	3.2±0.8	6.10	−0.18
Pels 66	1.0	4.9±0.8	7.39	0.45	Pels 189	0.93	4.9±0.8	5.87	0.53
Pels 71	0.77	11.1±0.9	6.25	0.23	Pels 192	1.34	11.4±0.9	6.77	0.34

less than 1 km s^{-1} down to $v \sin i$ 3 km s^{-1}. The standard deviation of the $v \sin i$ difference 1.4 km s^{-1} is in agreement with the combined error estimate. This strengthens the reliability of our results and clearly pushes our $v \sin i$ detection limit down to 3 km s^{-1}. Since both sets of data are coherent, they have been merged together. When two measurements are available for the same star, a weighted mean is computed.

The resulting $v \sin i$ distribution of low-mass Pleiades stars is shown in Fig. 4. The ELODIE and CORAVEL samples were supplemented with published $v \sin i$ measurements (Soderblom et al. 1993) when the star was not observed by ELODIE or

CORAVEL or when it was detected as a fast rotator with only a CORAVEL lower limit. The data displayed in Fig. 4 represents the $v \sin i$ sample used in the data analysis below to compute the distributions of equatorial velocity in Pleiades. Note that the following Pleiades stars are excluded for the data analysis: HII 761, HII 1338, HII 2407. They are all short period binaries with rotation rates synchronized with their orbital motions (Mermilliod et al. 1992; Raboud & Mermilliod 1998). Their rotation rate is driven by the tidal interaction between each components instead of by the angular momentum history of each star itself.

The comparison between $v \sin i$ measurements and period measurements provides an external check on our calibration. There are 19 slow rotators ($v \sin i < 15\,\mathrm{km\,s^{-1}}$) in our sample with known rotational periods (Prosser et al. 1995; O'Dell et al. 1995; Krishnamurthi et al. 1997b). We find that the resulting $\sin i$ distribution ($v \sin i / v$) is consistent with a random $\sin i$ distribution.

We may expect the turbulence in the atmosphere of the young stars to be larger, than for the old ones – the calibrators –, despite that there is no prove of it but only arguments related to a possible extra stirring-up in the photosphere of chromospherically active stars (spots). This effect would make us to over-estimate all $v \sin i$ measurements of slow rotators. However, since nothing significant has been detected by the comparison with period measurements, such effect, if real, has to be very small. We are aware that such a small comparison sample still leaves large statistical uncertainties but any systematic effects what would systematically change the $v \sin i$ value of slow rotators by more than $1\,\mathrm{km\,s^{-1}}$ can be ruled out.

The $v \sin i$ distribution of the corona stars compared to that located in the center does not show any significant differences excepted perhaps in the $0.77 - 0.94$ $(B-V)_0$ range where a slight excess of slow rotators might be seen in the corona (see on Fig. 4). In this $(B-V)_0$ range, the K-S statistical test indicates a probability of 96% that the difference between the $v \sin i$ distributions of the corona and the core of cluster is real. It may thus be that some of the slowest rotators in this $(B-V)_0$ range are not Pleiades members since we do expect a few field stars to contaminate our corona sample (see above). At this point, this difference cannot be interpreted as an intrinsic difference between the rotational velocity distributions of corona and core stars.

Finally, for the sake of completness, Table 6 lists stars identified in the literature as probable Pleiades member but whose radial velocity is found here to conflict with membership. We consider these stars as non-members. For the 3 Pels objects, this is a somewhat conservative conclusion since we only have one velocity measurement. A second measurement at least is necessary to exclude SB1 and draw conclusions on their membership. However, the very small $v \sin i$ values of these 3 stars is an extra indication that they are likely to be field stars.

3. Rotational velocity distribution

A numerical method is used to derive the distribution of equatorial velocities from the complete sample of $v \sin i$. We use the statistical relationships between the projected rotations and the equatorial rotations derived by Chandrasekhar & Münch (1950), and the numerical inversion procedure developed by Gaigé (1992).

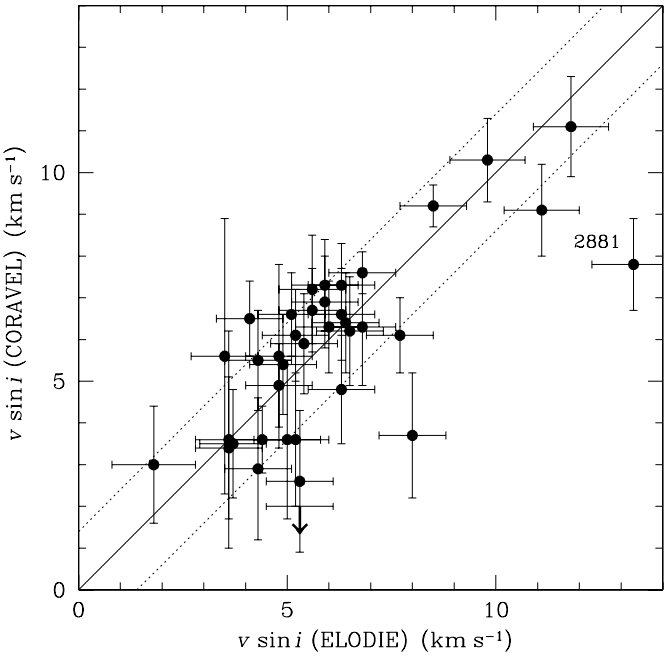

Fig. 3. Comparison between ELODIE and CORAVEL $v \sin i$ measurements of Pleiades stars. The solid line indicates the one-to-one relation and the dotted lines $\pm 1.4\,\mathrm{km\,s^{-1}}$. Both data sets show a very good agreement excepted for HII 2881. However this star is suspected to be an unresolved SB2. It is a close visual binary (Bouvier et al. 1997a) and the CORAVEL data show a radial velocity variability and changes of the width of the cross-correlation function over few years.

Table 6. New stars detected as non-members of Pleiades.

star	V_r (km s^{-1})	JDB	$v \sin i$ (km s^{-1})
Pels 93	-31.2	50394.7	< 2
Pels 117	11.1	50394.4	2
Pels 132	24.9	50394.6	< 2
HII3030	-.7	49752.4	< 2
	-.4	50394.5	< 2

3.1. Procedure description

Chandrasekhar and Münch (1950) first expressed the analytical relationships between the distributions of projected and equatorial velocities, under the assumption that rotational axes are randomly distributed in space. With $y = v \sin i$, its distribution $\phi(y)$ is related to the distribution of equatorial velocities $f(v)$ by:

$$\phi(y) = y \int_y^\infty \frac{f(v)}{v(v^2 - y^2)^{1/2}} dv, \qquad (3)$$

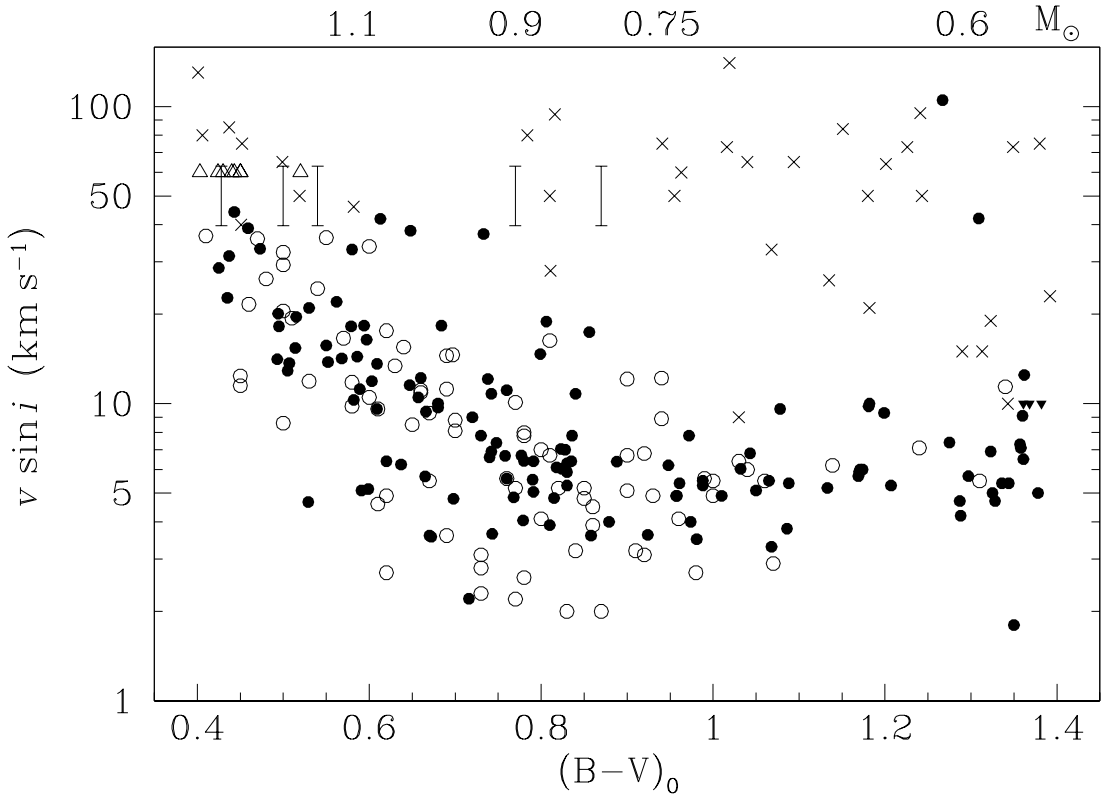

Fig. 4. $v \sin i$ of Pleiades stars with spectral type ranging from F5 to M0. Measurements from this work are displayed as circles. The filled circles represent stars within a distance of $80'$ from the cluster's center and the open circles are stars in the Pleiades corona ($r > 80'$). The crosses represent measurements from other sources (see Soderblom 1993). The triangles indicate unresolved $v \sin i$ (head-up: lower limit, head-down: upper limit). The error bars are used for CORAVEL measurements with large $v \sin i$ where systematic effects decrease the accuracy of the measurements (see text for explanations). The binary systems which are synchronized by tidal effects are not displayed.

and

$$f(v) = -\frac{2}{\pi} v^2 \frac{\partial}{\partial v} v \int_v^\infty \frac{\phi(y)}{y^2 (y^2 - v^2)^{1/2}} dy. \quad (4)$$

In order to solve the inverse problem, i.e., to compute $f(v)$ from $\phi(y)$ from Eq. 4, the (non continuous) distribution of projected velocities has to be differentiated. Chandrasekhar and Münch suggested that it would be easier to first assume a parametric form for $f(v)$, then to compute the corresponding $v \sin i$ distribution (direct problem) and finally adjust a set of parameters to reproduce the observations. But this method requires assumptions on the a priori unknown shape of $f(v)$. The large number of $v \sin i$ resolved in the Pleiades allow us instead to use a numerical inversion method to measure $f(v)$ from $\phi(y)$.

The numerical computation of Eq. 4 requires that $\phi(y)$ be a continuous fonction. In order to transform the observed distribution into a continuous function, we suppose that the contribution of each $v \sin i$ measurement (y_i) to the final distribution $\phi(y)$ can be modeled by a Gaussian-shape distribution probability $p_i(y) = 1/(l\sqrt{2\pi}) \exp(-(y - y_i)^2/(2l^2))$, centered in y_i and with l the σ–width of the Gaussian (Gaigé 1992). In other words, each measurement is "distributed" over a $v \sin i$ range with a Gaussian probability. Under this assumption, the distribution of projected velocities becomes a continuous function formed by a sum of Gaussians:

$$\phi(y) = \frac{1}{N} \sum_{i=1}^{N} p_i(y), \quad (5)$$

with N the number of measurements. With these assumptions, Eq. 4 is finally solved using standard differentiation and integration algorithms (see Gaigé 1992 for details).

In addition, we define the cumulative distributions both for projected and equatorial velocities:

$$\Phi(y) = \int_0^y \phi(x) dx \quad , \quad F(v) = \int_0^v f(w) dw$$

3.2. Tests on the stability on the inversion procedure.

The detailed shape of the inverse distributions $f(v)$ and $F(v)$ depends upon the number of stars N, and on the width of the Gaussian l used to transform the observed projected distribution into a continuous one. In order to test the stability of the inversion procedure and to investigate the influence of l and N, we have run Monte-Carlo simulations starting from a synthetic initial equatorial velocity distribution $f_0(v)$. This distribution has been chosen so as to mimic the observed distribution in the Pleiades:

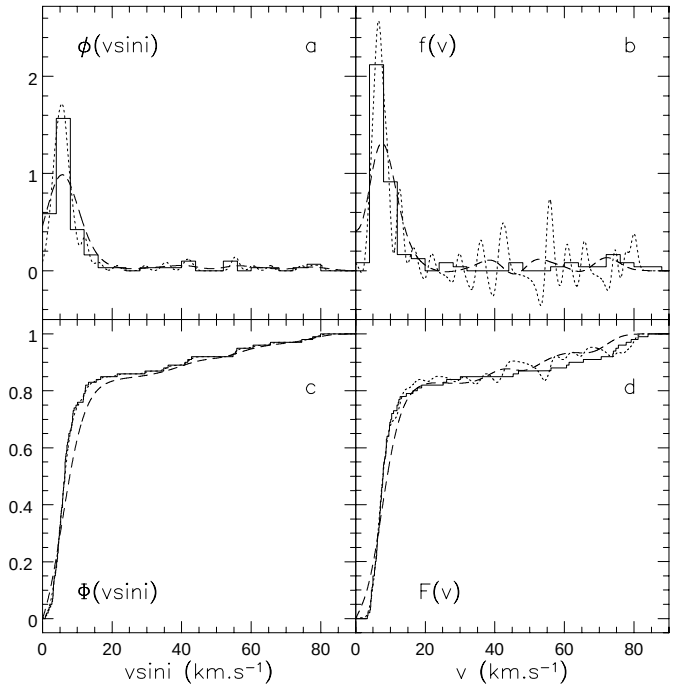

Fig. 5a–d. Example of the influence of the parameter l on the inversion procedure and the measurement of the rotational velocity distribution for a sample of 100 measurements. **a** solid line histogram displays a simulated projected velocity distribution computed from the $f_0(v)$ distribution showed in panel b. The continue estimation $\phi(y)$ is displayed with dotted line for $l = 1\,\mathrm{km\,s^{-1}}$ and dashed line $l = 4\,\mathrm{km\,s^{-1}}$. **b** solid line histogram indicates initial velocity distribution $f_0(v)$. Dotted and dashed lines show the final result after the Monte-Carlo simulation for repectively $l = 1\,\mathrm{km\,s^{-1}}$ and $l = 4\,\mathrm{km\,s^{-1}}$. **c-d** same than a and b panels but the cumulative distributions are displayed.

a peak at low velocity and a high-velocity tail. The steps of our Monte-carlo simulation were the following: First we generated a sample of N equatorial velocities v_i distributed along $f_0(v)$. Second, a random $\sin i$ was applied to each velocity to simulate an observed projected rotational velocity y_i. Third we computed the continue velocity distribution $\phi(y)$. Finally we solved Eq. 4 and we got a measurement of the equatorial velocity distribution $f(v)$.

As a first order test we have run this simulation for a large number of measurements (1000). In all cases, the "measured" equatorial rotational velocity distribution $f(v)$, was equivalent to the original $f_0(v)$. It means that the inversion procedure is robust and does not introduce systematic biases in the final result. We proceed by investigating the influence of l and the sample size (N) with the same Monte-Carlo method. We used various values of N between 20 and 200 and two values of l: 1 and 4 $\mathrm{km\,s^{-1}}$. In Fig. 5 we display the result of these simulations for $N = 100$.

Regardless of the sample size, the peak of the synthetic $\phi(y)$ distribution is well fitted using a small value of l, while for larger l the agreement is poor. For the high-velocity tail, where the number of stars is small, oscillations tend to develop for low-N and low-l values. The main issue is thus to determine the correct value of l, as a function of N, which yields a good fit to the original distribution. On the one hand, a small value of l leads to unrealistic fluctuations in the fit of the $\phi(y)$ distributions, especially for the tail of fast rotators. On the other, a large l value leads to a much smoother curve which does not reproduce well the sharp low-velocity peak. The high-velocity tail is better reproduced with a large l value and the details of the low-velocity peak with a smaller value of l .

Cumulative distributions are less sensitive to the parameter l. For a given rotation value, the frequency distribution is sensitive to the number of stars in the bin-width l centered on this value, while cumulative distribution depends only on the sum of projected or equatorial rotational velocity up to this value. In all cases, a small l, leads to a better match of the cumulative distributions.

The inversion of both curves ($\phi(y)_{l=1}$ and $\phi(y)_{l=4}$) is displayed on Fig. 5b and d. Statistical fluctuations are amplified by the numerical inversion leading to important differences between the two curves. For small l, the frequency distribution can even take unphysical negative values in the high-velocity tail, leading to a local decrease of the cumulative distribution.

In summary, two main factors have lead to the selection of the best value of l: the number of measurements and the shape of the $v \sin i$ distribution. In the case of the Pleiades, the observed distribution shows a sharp peak at low velocities, and an extending tail to the rapid rotators (see on Fig. 6). With the large numbers of slow rotators and the high precision of $v \sin i$ measurements one can use a small l in this domain. On the contrary, the small number of fast rotators requires a large value of l. Therefore we decided to use a l parameter which scales upon $v \sin i$ as $l \approx 0.2\, v \sin i$, with a minimum of 0.8 $\mathrm{km\,s^{-1}}$ for small rotators and a maximum of 10 $\mathrm{km\,s^{-1}}$ for large $v \sin i$ (these values might slightly vary from one mass bin to another). In addition we have imposed a lower limit of 1.5 $\mathrm{km\,s^{-1}}$ on the value of l corresponding to the errors on $v \sin i$ measurements for slow rotators. Our results displayed on Fig. 6 indicates that this choice is fairly good.

4. Equatorial rotational velocity distributions in the Pleiades

The distributions of projected velocities observed in the Pleiades are fitted and inverted using the inversion procedure described in the previous section. Since all $v \sin i$ are resolved and we have a complete sample free of any selection effect up to $(\mathrm{B-V})_0 = 1.3$, the equatorial velocity distributions for various mass ranges in the 0.6-1.4 $M_\odot$ domain can be measured. Table 7 lists the mass bins within which the inversion was performed and the corresponding number of measurements. The sample below 0.6 $M_\odot$ ($(\mathrm{B-V})_0 > 1.29$) is not complete and is biased towards the moderate rotators by some $v \sin i$ upper limits. The statistical results computed for this mass range have to be taken with caution.

The cumulative distributions of equatorial velocities for each bin of mass are displayed in Fig. 7. They show very different shapes between each others. Among the stars with masses

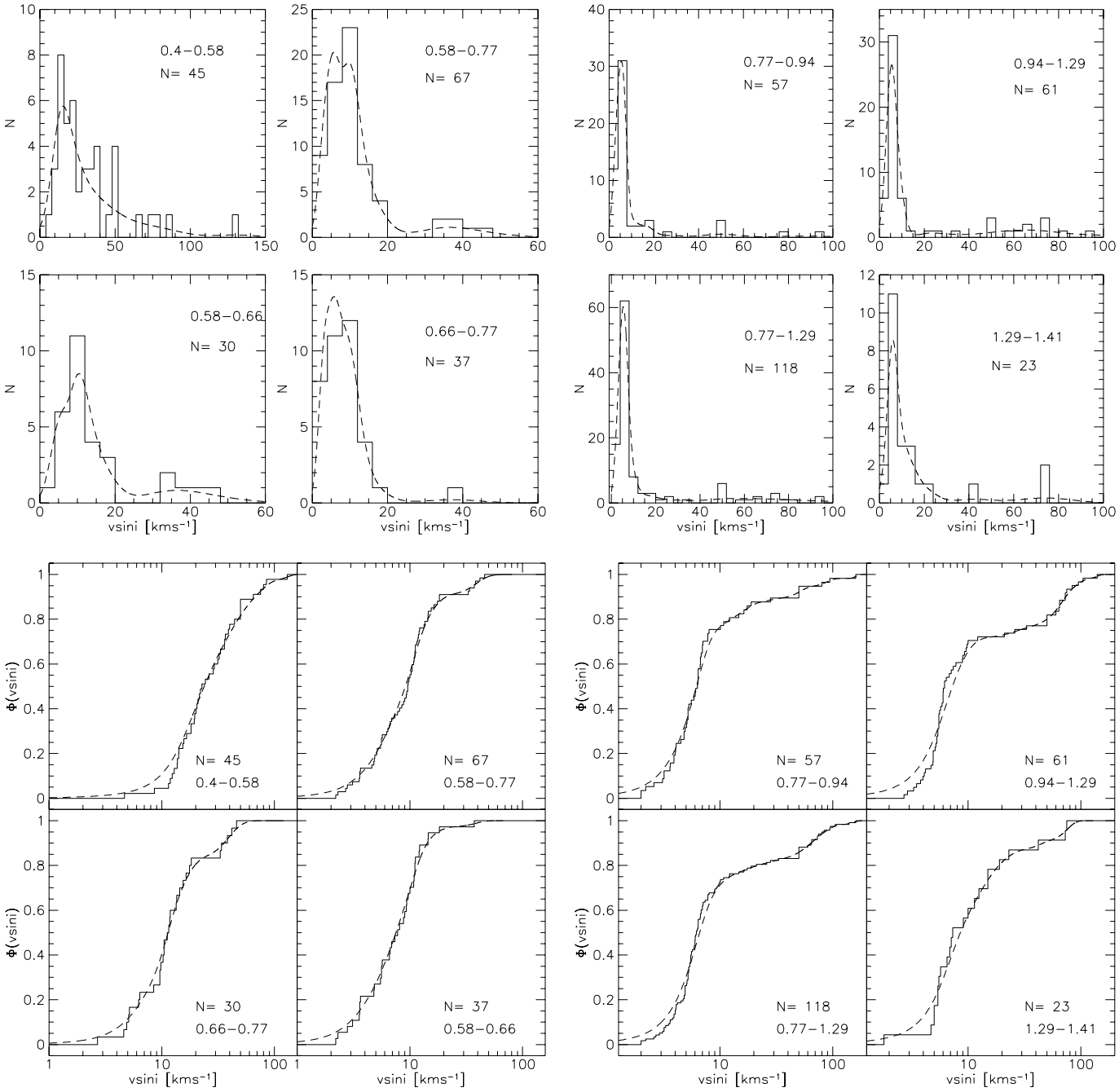

Fig. 6. Upper panels Histograms of observed $v \sin i$ distributions for all selected mass domains (displayed in $(B-V)_0$ ranges) and their fitted continuous distributions (dashed) which is used in the inversion process. **Lower panels** similar but the cumulative distributions are displayed.

above 1.1 $M_\odot$ there are no slow rotators. Below $1M_\odot$, the fraction of slow rotators dramatically increases and most of them have an equatorial velocity less than 15 $\mathrm{km\,s^{-1}}$. The smallest fraction of fast rotators (≥ 20 $\mathrm{km\,s^{-1}}$) is measured in the 0.9–1.0 $M_\odot$ mass bin. But the highest ratio of very slow rotators (≤ 10 $\mathrm{km\,s^{-1}}$) is observed for K dwarfs. About half of stars with a mass between $0.75M_\odot$ and $0.9M_\odot$ have rotations less than $7.5\,\mathrm{km\,s^{-1}}$ or $\Omega < 5\Omega_\odot$.

In order to check if there is any difference between the velocity distributions in the core and in the corona (stars located at a distance larger than 80' away from the center), we computed distributions for both samples separately. For all the wide mass ranges studied (0.6–0.9, 0.9–1.1, 1.1–1.5 $M_\odot$) no significant difference was found between the corona and the core. However in the 0.75-0.9 $M_\odot$ sub-range a slight excess of slow rotator is found in the corona compared to the core. We interpret this difference as the result of a contamination of our data by a few non–members. Indeed, after having rejected the 2 slowest rotators no significant difference remains between the two distributions. Considering the size of our samples and the small number of non-members foreseen from the selection process,

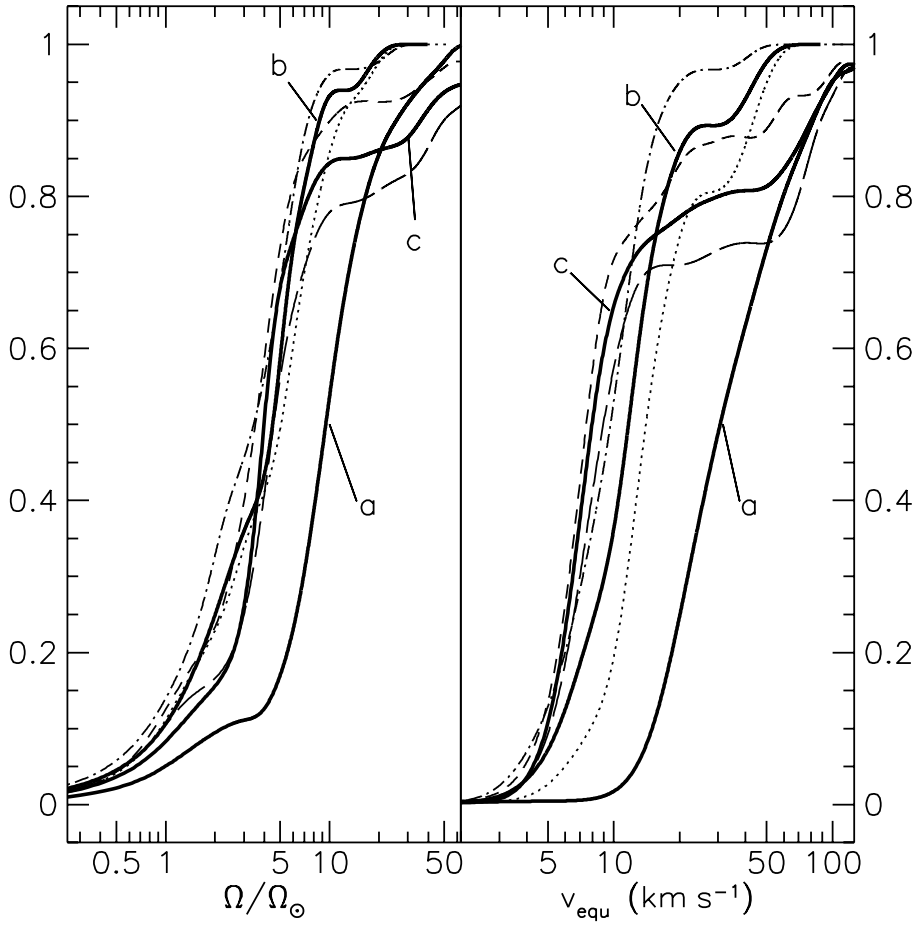

Fig. 7. Cumulative distributions of the equatorial ($V_{\rm equ}$) and angular ($\Omega/\Omega_{\odot}$) velocity in Pleiades for various mass domains ($M_{\odot}$). Wide bins : **a** 1.1 – 1.5, **b** 0.9 – 1.1, **c** 0.6 – 0.9. Narrow bins: (dot) 1.0 – 1.1, (dot–dash) 0.9 – 1.0, (short dash) 0.75 – 0.9, (long dash) 0.6 –0.75.

we expect that the contamination will not significantly affect the conclusions that we have derived.

In order to set reliable constraints for the modeling of angular momentum evolution of stars, we have computed the error bars on the cumulative distributions due to the finite number of measurements used. For each mass bin we have first randomly generated a synthetic set of equatorial rotational velocities equal to the number of $v \sin i$ measurements carried out and statistically distributed along the inverted distribution $f(v)$. We have multiplied each rotational velocity by a random value of $\sin i$ in order to get a simulated set of "observed data". We have finally applied our inversion procedure to derive a reconstructed $f(v)$ distribution. By repeating this process many times (100) we obtain an estimate of the statistical noise affecting our final distributions. The resulting 1σ error bars are listed in Table 7.

5. Discussion

5.1. Comparison with others clusters

The Hyades cluster is an excellent comparison cluster. It is older, its members are well known and rotational periods have been measured for numerous stars over a mass domain starting from late F up to late K (Radick et al. 1987). From G to early K the rotators show very small scatter per mass domain, so that it is possible to define a single mass-rotation sequence and use it as a reference. Few others clusters have such a complete sample of rotational data carried out without any selection or observational bias. In M 34, IC 2391 and IC 2602 recent measurements have been collected respectively by Jones et al. (1997) and Stauffer et al. (1997b). The G dwarf samples in these clusters only include part of the cluster stars but according to these authors they are free of any significant observational bias towards fast rotators, such as X-ray selection. The contamination of M34 candidate members by field stars is likely higher than in IC 2391 and IC 2602 and its slow rotators barely resolved. Nevertheless, because the age of M 34 is so critical to characterize the evolution of rotation in late-type dwarfs, we have decided to retain this set of data. For our analysis we consider that all these clusters can be used as an age sequence to track the evolution of the rotation of the slow rotators before and after the Pleiades age. We use the median of the rotational velocity distribution ($F(v) = 50\%$), a kind of upper limit for the slow rotators distribution, as a statistical indicator of the behavior of this population. This indicator, contrary to the mean, does not depend on the exact value of rotation for the smaller rotators. It is also little affected by the incompleteness that could arise from a few very-fast rotators which could have been missed or which have spectral lines too much broadened to measure reliable $v \sin i$. For M34, IC 2391 and IC 2602 clusters, the median of the velocity distributions is estimated from the median of $v \sin i$ distributions divided by

Table 7. Statistics on the distribution of the rotational velocity in Pleiades for each mass domain selected: N is the number of stars in the mass bin considered. In the upper part of the table, the percentages of stars with velocities less than 20, 10, 7.5 and 5 km s^{-1} are listed in each mass bin. In the lower part, the equatorial velocity v corresponding to various values of the cumulative distribution is indicated. See the text for explanations about the error bar estimates.

$(B-V)_0$	Mass	N	Fraction of stars (in %) with			
range	$M_\odot$		v <20 km s^{-1}	v <10 km s^{-1}	v <7.5 km s^{-1}	v <5 km s^{-1}
0.4 – 0.58	**1.1 – 1.5**	45	24.6±5.4	1.7±2	0.6±1.3	0.4±0.7
0.58 – 0.77	**0.9 – 1.1**	67	85.8±4.6	36.1±6.1	21.3±7.1	7.1± 3.6
0.58 – 0.66	1.0 – 1.1	30	74.6±8.4	19.4±8.6	9.1±5.7	2.7± 3.1
0.66 – 0.77	0.9 – 1.0	37	94.9±3.7	52.9±10.0	32.3±9.2	12.8±5.9
0.77 – 1.29	**0.6 – 0.9**	118	77.3±3.7	65.5±4.1	44.0±3.9	10.6±2.9
0.77 – 0.94	0.75 – 0.9	57	84.2±4.1	71.6±5.3	50.2±5.7	13.4±4.7
0.94 – 1.29	0.6 – 0.75	61	71.0±6.2	57.4±5.1	35.3±4.9	9.1±3.4
1.29 – 1.41	**0.5 – 0.6**(†)	23	76.4±9	45.7±9.5	26.5±7.7	5.6± 4.9
			velocity v (km s^{-1}) such that			
			$F(v)$ <10%	$F(v)$ <20%	$F(v)$ <50%	$F(v)$ <90%
0.4 – 0.58	**1.1 – 1.5**	45	14.9±2.1	18.4±1.9	30.6±2.7	82 ± 11
0.58 – 0.77	**0.9 – 1.1**	67	5.5 ±1.0	7.2±0.9	11.6±0.9	34 ± 8
0.58 – 0.66	1.0 – 1.1	30	7.8 ±1.3	10.1±1.2	14.0±1.7	44 ± 10
0.66 – 0.77	0.9 – 1.0	37	4.5 ±1.0	6.0±0.9	9.6±1.0	16.1±3.3
0.77 – 1.29	**0.6 – 0.9**	118	4.9 ±0.4	5.8±0.3	7.9±0.4	80 ± 13
0.77 – 0.94	0.75 – 0.9	57	4.6 ±0.5	5.5±0.4	7.5±0.4	53 ± 23
0.94 – 1.29	0.6 – 0.75	61	5.0 ±0.5	6.1±0.5	8.9±3.3	89 ± 13
1.29 – 1.41	**0.5 – 0.6**(†)	23	5.6±1.0	6.8±1.0	10.8±2.0	72 ± 25

(†) The selected sample in this mass range suffers from incompletness. The number of slow rotators is underestimated. The fraction of stars with $v < 7.5$ km s^{-1} and $v < 5$ km s^{-1} are only lower limit estimates.

$4/\pi$. Monte–Carlo simulations show that this rough correction is accurate enough (10% difference) if the velocity distribution has a similar shape to that measured in the Pleiades for the $0.58 <(B-V)_0< 0.77$ domain.

The comparison between these clusters is shown in Fig. 8. It indicates that 50% of the Pleiades G and K dwarfs have a rotation rate at most about twice as large as that of Hyades dwarfs. With an age of 100 Myr for the Pleiades (see Basri et al. 1996 for a very complete discussion of this value), and an age of 600 Myr for the Hyades, this would lead to $\Omega(t) \approx t^{-\alpha}$, with $\alpha < 0.3$ instead of the canonical 0.5 exponent of Skumanich's (1972) relationship. Since the G dwarfs and early K dwarfs do not contract any more beyond 100 Myr, their angular momentum evolution is only driven by losses from stellar wind and, possibly, the resurfacing of the (faster) core rotation. The small value of the exponent that we find for the Skumanich-type power-law above is therefore an indication that either the braking of moderate rotators is less efficient than predicted by the asymptotical Skumanich's relationship ($dJ/dt \propto \Omega^3$) or that some recoupling between the core and envelope occurs between the age of the Pleiades and the Hyades age, with the fast spinning core transferring angular momentum to the envelope.

The 10% slowest rotators of the Pleiades have rotation rates quite similar to those of Hyades dwarfs. If we scale the rotational behaviour of moderate rotators from Pleiades to Hyades to this population of very slow rotators, we would expect to find some stars in the Hyades with rotation periods similar to the Sun. Even though this seems to conflict with current data on the rotation of late-type dwarfs in the Hyades, the relatively small sample studied by Radick et al. (1987) does not preclude the existence of 10% or so extremely slow, solar-type rotators in the Hyades.

IC 2391 and IC 2602 are both very young clusters of about 35 Myr and their G dwarfs have just arrived on the main sequence. The G dwarf sample in these clusters therefore provides an estimate of the rotational distribution on the ZAMS. The median rotation rate observed in these clusters agrees well with the value predicted by Skumanich's relationship applied backwards in time starting from the Pleiades and assuming solid body rotation. This suggests that these rotators experience non-saturated braking[1], i.e., $dJ/dt \propto \Omega^3$. Since the median velocity of Pleiades and Hyades dwarfs is even lower than that of IC cluster dwarfs, they too must lie in a regime where the angular

[1] We refer to "saturated" and "non-saturated" breakings as the two different breaking laws usually used in the angular momentum models for respectively fast and slow rotators. Discussions and references regarding the link between the observed saturation of the activity indicators for fast rotators (see Sect. 5.2) and the suggested saturation of the breaking laws can be found in Bouvier et al. (1997)

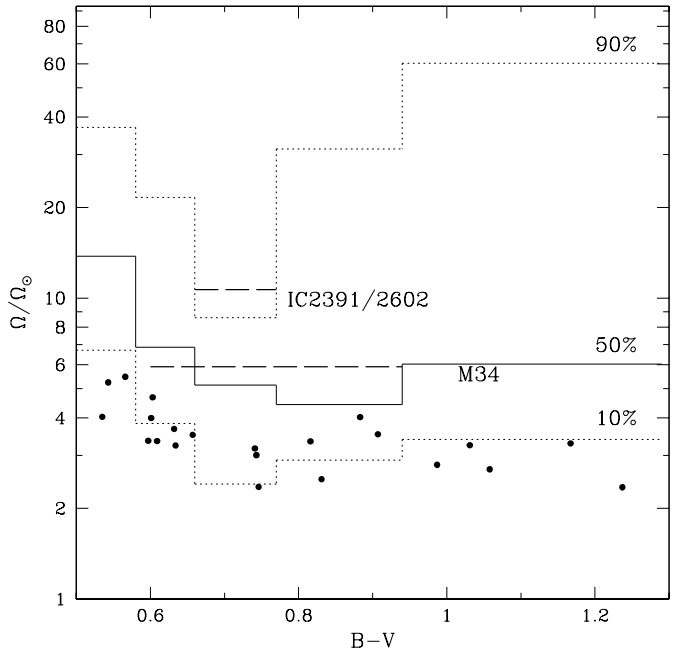

Fig. 8. Rotational velocity distribution of the Pleiades compared to that of the Hyades, M34 and IC2391/2602. The dots represents the individual rotation period measurements of Hyades dwarfs converted to angular velocity. The median of the rotational velocity distribution for the Pleiades $F(< 50\%)$ and two border value $F(< 10\%)$ and $F(< 90\%)$ are displayed by solid and dotted lines. Dashed lines indicates the median of the velocity distribution for G-dwarfs for both young clusters IC 2391, IC 2602 and M34 computed from their $v \sin i$ cumulative distributions and corrected by $4/\pi$.

momentum losses are not yet saturated, which occurs at about $25\,\mathrm{km\,s^{-1}}$ for solar type stars (see Sect. 5.2). If a "partially-saturated" braking regime had occurred between the IC clusters and the Pleiades, we would have observed more fast rotators in the Pleiades. Similarily, recoupling of the fast rotating core with the slow rotating envelope earlier than Pleiades is also unlikely since in this case a faster median rotation would have been measured in the Pleiades. Altogether, the evolution of the median velocity from the Pleiades to the Hyades is then best understood as the result of angular momentum from the core resurfacing into the envelope within this few 100 Myr time span.

The median rotation rate of G and early K dwarfs in the M34 cluster is slightly higher than the Pleiades one. According to Jones et al. (1997), contamination by field stars can be expected in the M34 sample, which would underestimates the true median velocity. Since M34 is older than Pleiades –between 180 Myr (Meynet et al. 1993) and 250 Myr (Jones et al. 1997)–, this result does not fit immediately into the paradigm of the continuous braking of stellar rotation with time on the main sequence. The different ages assigned to M34 by Jones et al. (1997) and Meynet et al. (1993) mostly result from the use of different reddening corrections: 0.07 in the former, and 0.11 in the latter. A reanalysis of Geneva photometric measurements and UBV data tends to favor a higher reddening and the Meynet et al. (1993) age of 180 Myr. The age difference between Pleiades and M34 could thus be sufficiently small so that the rotational distributions would look somewhat similar. In addition, there is some uncertainty on the value of G dwarf median rotation velocity of M34 due to the small number of observations carried out (18). However, the nearly equal median velocities measured for G dwarfs in the Pleiades and in M34 can be readily understood if resurfacing of core angular momentum into the convective envelope occurs on a time scale of about 100 Myr.

These results thus provide a coherent global picture for the observed evolution of the median velocity of G dwarfs from 35 Myr to 600 Myr, which strongly suggests that, for slow and medium rotators, the initially fast rotating radiative core transfers angular momentum to the convective envelope on a timescale of 100–200 Myr. This work does not set any constraint on the coupling time for fast rotators.

An alternative to the core-decoupling interpretation would be to assume that the rotational distribution on the ZAMS differs from cluster to cluster. The spread in initial angular momentum builds up during the pre-main sequence as the star is still locked to its circumstellar disk. Any difference in the disk-lifetime distribution between clusters would thus lead to different ZAMS velocity distributions. In such a case, the early velocity distribution would be primarily driven by the physical parameters of the proto–stellar local environment and not by the age of clusters. Moreover the subtle effects of metallicity and binary content upon angular momentum losses are not yet elucidated. However, there is currently no evidence that these effects can strongly impact upon the angular momentum evolution of young low-mass stars. For instance, both single and binary G and K dwarfs in the Pleiades appear to follow the same rotational velocity distribution (Bouvier et al. 1997a). Pending evidence that other processes than those currently included in the models can affect the angular momentum evolution of young stars, our results favor the hypothesis of core-envelope recoupling during the early main sequence evolution.

5.2. The activity–rotation connection

Since the pioneering work of Kraft (1967), many studies have been carried out about the relation between the rotation and the activity of stars. It is now obvious that both the chromospheric and the coronal emission is tightly linked to the stellar rotation and to the depth of the stellar convection zone –or convective turnover time τ_c– and such a relationship is consistent with the qualitative predictions of the $\alpha\omega$-dynamo magnetic field generation.

The recent ROSAT observations of nearby open clusters have boosted our knowledge about the X-ray emission of young stars (see Caillault 1996, for references). The best way to display the connection between the magnetic field generation and the stellar activity is probably the Rossby diagram (activity indicator versus Rossby number R_0). Noyes et al. (1984) has clearly shown, using the Ca H-K lines as an activity indicator, that such a diagram allows one to combine stars with a wide range of mass without significantly increasing the dispersion.

When the Rossby diagram is displayed for dwarf stars with spectral types between F5 to M5, using $\log(L_{\rm X}/L_{\rm bol})$ as the coronal activity indicator, it shows an obvious discontinuity near $\log(N_R) \approx -.75$. On the one hand, for the rapid rotators, a "saturation plateau" suggests an upper limit of about $\log(L_{\rm X}/L_{\rm bol}) \approx -3$. On the other hand, for slow rotators – Hyades and most field stars–, $\log(L_{\rm X}/L_{\rm bol})$ steadily decreases when the Rossby number increases (see for examples Patten & Simon 1996; Randich et al. 1996). The exact location of the transition between the saturated and unsaturated regimes is still ill-defined due to the lack of precise rotation measurements for rotators in the 5 to 15 km s^{-1} range. Most of the G and K dwarfs in the Pleiades have rotation rates less than 20 km s^{-1} and therefore lie around the transition zone between the "saturation plateau" and the slow rotators in the Rossby diagram. They thus provide an opportunity to fill a scarce populated region of the Rossby diagram.

To build a Rossby diagram with our Pleiades data, we have converted our $v \sin i$ measurements into a $v \sin i$-based Rossby number: $\log(R_0/\sin i) = \log(P/\tau_c) - \log(\sin i) = \log(P/\sin i) + \log(1/\tau_c)$, where $P/\sin i$ is derived from $v \sin i$ using the radius–(B−V)$_0$ calibration of Schmidt-Kaler (1982) and the turnover time τ_c is computed from Eq. 4 of Noyes et al. (1984). The cumulative distribution of $\log(\sin i)$ is a very steep function around zero with a mean of -0.13 and a 90% probability to have $\log(\sin i) > -.38$. The spread in the Rossby diagram induced by the $\sin i$ distribution alone is less than the spread observed for Hyades and field stars at a given $\log(L_{\rm X}/L_{\rm bol})$ value in this diagram. The $\sin i$ statistics therefore merely introduces a bias in the diagram by systematically shifting the data towards higher Rossby numbers. The distribution of $\log(\sin i)$ is strongly skewed. Quite often in the literature, individual $v \sin i$ measurements are transformed into $V_{\rm equ}$ by multiplying $v \sin i$ by the average factor $4/\pi$. However, this correction is valid only for the mean rotational velocity and cannot be applied to individual measurements.

On Fig. 9 the Rossby diagram is displayed for all Pleiades dwarfs with $0.5 <$(B−V)$_0< 1.4$ and X-ray measurements from ROSAT PSPC imager. All known binaries have been rejected. As expected, the Pleiades data lie around the transition zone. Taking into account the statistical shift and the spread arising from the $v \sin i$–based Rossby number, the Pleiades data perfectly link the slowly rotating field and Hyades dwarfs and the fast rotators on the X-ray plateau. The slope in the non-saturated regime is about -2 in agreement with earlier results and theorical arguments from Maggio et al. (1987) and Schmitt et al. (1985). In a recent work on Alpha Per, Randich et al. (1996) found a much flatter slope of about -1. This value was derived from a least-square fit based on a limited sample of slow rotators whose rotation periods were partly estimated from $v \sin i$ measurements. The χ^2-fitting only works on normal random distributed data but not on $\sin i$ distributed data. The net result of this misuse is to give too much weight to the few outlying low $\sin i$ stars, thus flattening the slope. Therefore the Randich et al. (1996) value for Alpha Per is much more a lower limit than a real estimate of the slope.

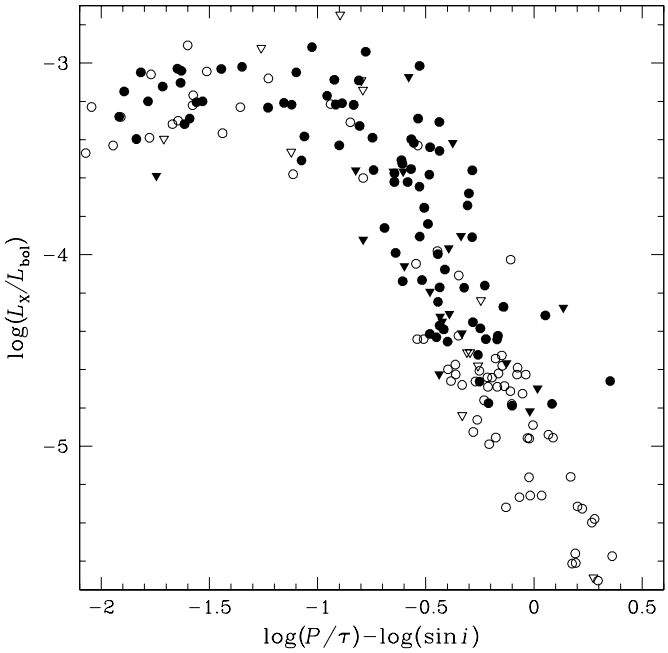

Fig. 9. Rossby diagram based on $v \sin i$ measurement of Pleiades stars with $0.5 <$(B−V)$_0< 1.4$ (filled symbols). All the known binaries have been rejected. The X-ray data are from Stauffer et al. (1994); Micela et al. (1996). Empty symbols represents stars from Alpha Per, Hyades and field stars whose rotational period has been directly measured ($\sin i = 1$ in this plot) and X-ray measurements come from ROSAT PSPC observations (data from Hempelmann et al. 1995; Randich et al. 1996 and Allain et al. 1997).

The transition zone lies at about $\log(P/\tau) = -0.8 \pm 0.1$, in agreement with a recent work from Stauffer et al. (1997b). The shape of the Rossby diagram is the same if we restrict the sample to limited mass ranges. The only effect is to shift the whole set of data towards the saturation plateau for stars with smaller masses. This effect is easily understood as these stars have deeper convective zone –and then larger τ_c– and include more fast rotators than higher mass stars. In conclusion, the Rossby diagram provides a coherent description of the rotation–activity connection in the mass range 0.5–1.2$M_\odot$. It shows that the saturation phenomenon is tightly linked to the stellar mass. Such a mass-dependent saturation effect had been previously suggested by Collier Cameron & Li (1994) and Barnes & Sofia (1996) and is confirmed here by Pleiades data.

6. Conclusions

From a complete and unbiased set of $v \sin i$ measurements, we have computed the distribution of equatorial velocities in the Pleiades for various mass ranges between 0.5 and 1.5$M_\odot$. Comparison with the distribution of rotational velocities in the Hyades, M 34, IC 2391 and IC 2602 yields a coherent picture for the angular momentum evolution of the convective envelope.

The comparison with the younger clusters IC 2391 and IC 2602 suggests that most Pleiades G–dwarfs are in an unsaturated braking law regime. The rotational evolution of moderate

rotators in early stages is in agreement with a solid body rotation driven by Skumanich's relationship. The relationship between $v \sin i$ and X-ray emission indicates that the transition between saturated X-ray emission and its steady decrease with rotation occurs at about $P = 2$ d or $v \sin i = 25\,\mathrm{km\,s^{-1}}$ for solar-type stars. About 10% of Pleiades G dwarfs lie in the saturation domain.

The comparison with older cluster such as M 34 and the Hyades strongly suggests that angular momentum of slow and moderate rotators is transported from the fast rotating core to the convective enveloppe on a time scale of about 100–200 Myr on the early main sequence. An alternative intepretation would call for intrinsic differences in the distribution of initial angular momenta from clusters to clusters, which is not currently supported by observations.

The advent, in the next decade, of multi-fiber spectrographs on large telescopes will offer the possibility of determining the $v \sin i$ distributions of more remote clusters of various ages and abundances as well as the rotational properties of very low-mass stars (0.1–0.5$M_\odot$). This will undoubtedly improve our understanding of the rotational evolution of young stars and provide new clues to the physical mechanisms responsible for angular momentum transport in stellar interiors.

Acknowledgements. We are grateful to S. Udry who kindly provided us his help for all operations with the CORAVEL database and to J. Stauffer, our referee, for his comments and his useful suggestions to improve the quality of the English. D.Q. acknowledges support from the swiss FNRS.

References

Allain S. Fernández M., Martín E.L., Bouvier J. 1997, A&A 314, 173
Allain S. 1998, A&A 333, 629
Arribas S., Crivellari L. 1989, A&A 210, 211
Artjukhina N.M., Kalinina E. 1970, Tr. Sternberg Astr. Inst. 39, 111
Baliunas S.L., Vaughan A.H., Hartmann L. et al. 1983, ApJ 275, 752
Baranne A., Mayor M., Poncet J.-L. 1979, Vistas in Astron., 23, 279
Baranne A., Queloz D., Mayor M., et al. 1996, A&A Suppl. Ser 119, 1
Barnes S., Sofia S. 1996, ApJ 462, 746
Basri G., Marcy G.W., Graham J.R. 1996, ApJ 458, 600
Benz W., Mayor M. 1981, A&A 93, 235
Benz W., Mayor M. 1984, A&A 138, 2183
Bouvier J. 1994, in Cool Stars, Stellar Systems, and the Sun, Eigth Cambridge Workshop, Jean-Pierre Caillault (ed.), ASP Conf. Ser. 64, 151
Bouvier J., Rigaut F., Nadeau D. 1997a, A&A 323, 139
Bouvier J., Forestini M., Allain S. 1997b, A&A 326, 1023
Caillault J.-P. 1996, in Cool stars, Stellar Systems, and the Sun, 9th Cambridge Workshop, Pallavicini and Andrea K. Dupree (eds.) ASP Conf Ser 109, 325
Camenzind A.C. 1990, in Rev. Modern Astronomy, G. Klare (eds.), 3, 234
Chandrasekhar S., Munch G. 1950, ApJ 111, 142
Choi P.I., Herbst W. 1996, AJ 111, 283
Collier Cameron A., Li J. 1994, MNRAS 269, 1099
Endal A.S., Sofia S. 1978, ApJ 220, 279
Gaigé Y. 1992, A&A 269, 267
Gray D. F. 1976, "The Observation and Analysis of Stellar Photospheres", Wiley & Sons Inc (eds.), New York.
Gray D.F. 1984, ApJ 281, 719
Hempelmann A., Schmitt J.H.M.M., Schultz M., Rüdiger G., Stepieǹ 1995, A&A 294, 515
Hertzprung E. 1947, Ann. Sterrewarte Leiden 19, No. 1A
Jones B.F., Fischer D., Shetrone M, Soderblom D.R. 1997, AJ 114, 352
Königl A. 1991, ApJ 370, L39
Kraft R.P. 1967, ApJ 150, 551
Krishnamurthi A., Pinsonneault M.H., Barnes S., Sofia S. 1997a, ApJ 480, 303
Krishnamurthi A., Terndrup D.M., Pinsonneault et al. 1997b, ApJ in press
Mac Gregor K.B., Brenner M. 1991, ApJ 376, 204
Maggio A., Sciortino S., Vaiana G.S. et al. 1987, ApJ 315, 687
Marcy G.W., Chen G.H. 1992, ApJ 390, 550
Mayor M., Mermilliod J.-C. 1991, in "Angular momentum evolution of young stars", NATA Workshop, S. Catalano and J.R. Stauffer (Ed.), Kluwer Publ. Co., Dordecht/Boston/Londo, 201
Mermilliod J.-C., Rosvick J.M., Duquennoy A., Mayor M. 1992, A&A 265, 513
Mermilliod J.-C., Bratschi P., Mayor M. 1997, A&A 320, 74
Meynet G., Mermilliod J.-C., Maeder A. 1993, A&AS, 98, 477
Micela G., Sciortino S., Kashyap V. Jr., Harnden F. R., Rosner R. 1996, ApJ Suppl. Ser. 102, 75
Noyes R.W., Hartmann L.W., Baliunas S.L., Duncan D.K., Vaughan A.H. 1984, ApJ 279, 763
O'Dell M.A., Panagi P., Hendry M.A., Collier Cameron A. 1995, A&A 294, 715
Patten B. M., Simon T. 1996, ApJ Supl. Ser 106, 489
Prosser C.F. 1992, AJ 103, 488
Prosser C.F., Shetrone M.D., Dasgupta A. et al. 1995, PASP 107, 211
Queloz D., 1995, in "New Developments in Array Technology and Applications", Davis Philip A.G. et al. (eds.), 221
Queloz D., Babel J., Mayor M. 1996, in 9th Cambridge Workshop, " Cool Stars Stellar System and the Sun", R. Pallavicini & A.K. Dupree (eds.), ASP Conf. Ser. 109, 627
Radick R.R., Thompson D.T., Lockwood G.W., Duncan D.K., Bagget W.E. 1987, ApJ 321, 459
Raboud Didier, Mermilliod J.-C. 1998, A&A 329, 101
Randich S. Schmidt J.H.M.M., Proser C.F., Stauffer J.R. 1996, A&A 305, 785
Rosvick J.M., Mermilliod J.-C., Mayor M. 1992, A&A 255, 130
Schatzmann E. 1962, Ann. d'Astrophys., 25, 18
Schmitt J.H.M.M., Golub L., Harnden F.R.Jr et al. 1985, ApJ 290, 307
Skumanich A. 1972, ApJ 171, 565
Smith M. A., Gray D. F., 1976, PASP 88, 809
Soderblom D. 1983, ApJ Suppl. Ser. 53, 1
Soderblom D.R., Stauffer J.R., Hudon J.D., Jones B.F. 1993, ApJ Suppl. Ser. 85, 315
Stauffer J.R., Caillaut J., Gagne M., Prosser C., Hartmann L. 1994, ApJ Suppl. Ser. 91, 625
Stauffer J.R., Balachandran S.C., Krishnamurthi A. et al. 1997a, ApJ 475, 604
Stauffer J.R., Hartmann L.W., Prosser C.F. et al. 1997b, ApJ 479, 776
Taylor B.J., Johnson S. 1987, ApJ 322, 930
Udry S. et al. 1998, in preparation
van Leeuwen F. 1983, Ph.D. dissertation (Leiden)
van Leeuwen F., Alphenaar P., 1982, ESO Messenger 28, 15
Weber E.J., Davis L. 1967, ApJ, 148, 217